

Preparation of Zinc-doped Titanium Dioxide Nanorod Arrays and Their Application in Dye Sensitized Solar Cells

D.S. Yao, Y.L. Zhao*, L. Zhu, J. Song, X.Q. Gu, J.J. Zhu, Y.H. Qiang

School of Materials Science and Engineering, China University of Mining and Technology, Xuzhou 221116, China

*E-mail: sdyulong@cumt.edu.cn

Received: 14 March 2015 / Accepted: 28 April 2015 / Published: 27 May 2015

Zn²⁺-TiO₂ nanorod arrays were prepared on fluorine-doped tin oxide (FTO) glass by thermal hydrolysis and applied as the anodic material of dye sensitized solar cells (DSSCs). Scanning electron microscopy (SEM), X-ray diffractometer (XRD) and X-ray photoelectron spectroscopy (XPS) were utilized to characterize their microstructures and components. The photoelectrochemical properties were detected by ultraviolet-visible spectroscopy (UV-VIS), photocurrent density-voltage measurement (J-V) and electrochemical impedance spectrum (EIS). The results of the above tests and characterizations showed that the TiO₂ nanorod arrays (TNRs) were monocystal with the rutile phase and doping Zn²⁺ in them strengthened absorbance intensity of visible light. Among these samples, the one doped by 2 mmol Zn²⁺ obtained the highest efficiency of 1.61% which was obviously promoted, compared with 0.8% of the standard sample prepared by pure TNRs.

Keywords: TiO₂ nanorod arrays; DSSCs; ion doping; thermal hydrolysis

1. INTRODUCTION

With the environmental-friendly and low-cost superiorities, dye-sensitized solar cells (DSSCs) have achieved remarkable energy conversion efficiency at the level of 12% and become one of the most promising substitutions to Si-based photovoltaic cells in recent twenty years [1-5]. Nevertheless, compared with relatively high efficiency as those of Si-based photovoltaic cells, bottlenecks of DSSCs in photovoltaic performance were mainly attributed to the high carrier recombination rates occurring at the interfaces [5, 6]. To overcome the disadvantage, TiO₂ nanorod arrays, which is considered to be one of the significant n-type semiconductor materials, provides uninterrupted electrical pathways for photogenerated electrons. Compared with several other morphological TiO₂ anodes for DSSCs such as TiO₂ polycrystalline or mesoporous films [7, 8], these structures have been proved to enhance the rate of

electron transport, results in high carrier collection efficiency and then improve the performance of DSSCs [9-16].

Nevertheless, the specific surface of TiO₂ nanorod arrays is quite smaller than that of TiO₂ nanoparticles, which results in poor dye absorption and low energy conversion efficiency [17-19]. Hence, how to adjust the microstructure and crystal interface of the TNRs to improve photoelectric performance has rise interest of scientists [20]. The study of ion doping in TiO₂ has been undertaken since 10 years ago. In recent researches, Nb-doped TiO₂ has already been applied in DSSCs [21-23]. According to the study reported by Lu et al. [24], 5 at% Nb-doped nanoparticles assumed a positive shift in a flat-band and effective electron injection, contributing to the advancement of nearly 20% in energy conversion efficiency [17]. Additionally, in order to form so-called semiconductor sensitized solar cells, CdSe and CdS nanocrystals have also been reported to coat TNRs successfully by chemical vapor transport [25], chemical bath deposition [26] and electrochemical deposition [27]. Meanwhile, 1.14% conversion efficiency has been achieved in CdS/CdSe co-sensitized solar cells [28]. All these research results demonstrate that doping proper components into TiO₂ is an effective way to improve the photoelectronic activity of TiO₂.

This study treated TiO₂ nanorod arrays by doping Zn²⁺ and aimed to seek the suitable ratio of them. Designed amounts of Zinc acetate was doping to the reaction solutions of tetrabutyl titanate (TBT) and hydrochloric acid after fully hydrolyzation. The influence of temperature, time, electrolyte concentration, and the photoelectric effect based on the microstructure and morphologies of the Zn²⁺-TNRs were also investigated.

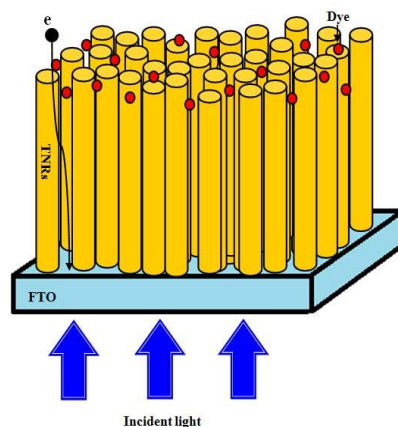
2. EXPERIMENTAL PROCEDURES

2.1 The preparation of Zn²⁺-TiO₂ nanorod arrays

The TNRs were prepared with a hydrothermal synthesis reported by Liu and Aydil [21]. Firstly, 15 mL concentrated hydrochloric acid (37 wt.%) was mixed with 15 mL deionized water. The mixed solution was stirred at room temperature for 5 min before 1mmol tetrabutyl titanate was added dropwise and at an extremely low rate. After a follow-up stir for 15 min, the solution was quartered and respectively added with 0 mmol, 1 mmol, 2 mmol and 3 mmol zinc acetate particles. After stirring for another 15 min, these four solutions were transferred to 4 autoclaves (100 mL volume) made from Teflonlined stainless steel. Pieces of FTO substrates (2 mm thickness, 14-20Ω/sq) were ultrasonically treated for 15 min in a mixed solution of isopropanol, acetone and deionized water with a volume ratio of 1:1:1 and then rinsed with ethanol for several times. They were placed in the inner autoclaves at an angle against the wall with the electric conducting side facing down. After that, the autoclaves were sent into an oven and the hydrothermal synthesis lasted at 150°C for 10 h. After cooling, the FTO substrates were taken out, rinsed with deionized water and dried in air. Finally, the selected four samples were gradually heated in a Muffle furnace under an air flow firstly at 325°C for 5min, then at 375°C for 5min, 450°C for 15min and at 500°C for 15 min.

2.2 DSSC assembly

After cooling to 80 °C, the sintered films were immersed into a 3 mmol ethanol solution of N719 (Dalian Hepta Chroma) for 24 h. Finally, typical sandwich-type solar cells with the dye-absorbed anodes and Pt-coated counter electrodes were assembled and sealed with 60 μm thick thermal-plastic surllyn (DHS-SN1760) spacer at 110°C for 15 s. The cells were then slightly clipped as an open cell and Scheme 1 showed the novel structure of TNRs photo anode. An iodide-based liquid electrolyte (0.6 M DMPII, 0.03 M I_2 , 0.5 M TBP and 0.1 M LiI in MPN, Dalian Hepta Chroma) was injected into the devices from the edge of the FTO glass and a thin layer of electrolyte formed in the inter-electrode space due to capillary forces. The cells were clamped and tested immediately.



Scheme 1. An illustration of the novel TNRs photo anode

2.3 Characterization

The morphology observation was operated by a field-emission scanning electron microscopy (FESEM, Hitachi, S-4800, Japan). The structural properties of the devices were characterized by X-ray diffraction (XRD, Bruker D8 Advance, Germany). The chemical components of these doped TiO_2 nanorod arrays samples were detected by X-ray photoelectron spectroscopy (XPS) on a Thermo ESCALAB250 XPS system. The UV-visible spectra of the Zn^{2+} - TiO_2 nanorod arrays were obtained using a spectrophotometer (UV-vis, Cary-300 spectrometer, 200-800 nm wavenumber, Varian). The photocurrent density–voltage (J-V) measurements were carried out under the 100 mW/cm^2 illumination, while the simulated sunlight of this system was provided by a 500W Xenon lamp fitted with an AM-1.5 fitter (Beijing Trusttech). Electrochemical impedance spectroscopy (EIS) analysis was made under illumination by using an electrochemical test station (CHI660D).

3. RESULTS AND DISCUSSION

3.1 Morphology and crystal phase analyses

Shown in Fig.1, compared with pure titanium dioxide nanorods, the morphology, diameter and even intensity of the Zn^{2+} doped TNRs under the same growth conditions do not obviously change,

which indicates doping Zn^{2+} in TNRs may not a simple process of mixing these two components but micro-scale of Zn^{2+} filling into the lattice of TNRs. This phenomenon above mentioned will be further confirmed by the XRD patterns.

The XRD patterns of pure TiO_2 nanorod arrays and Zn^{2+} -TNRs in Fig.2 shows the main diffraction peaks at 27.08° , 36.67° and 52.00° reflect the (110), (101) and (211) crystal indices of the rutile crystalline phase.

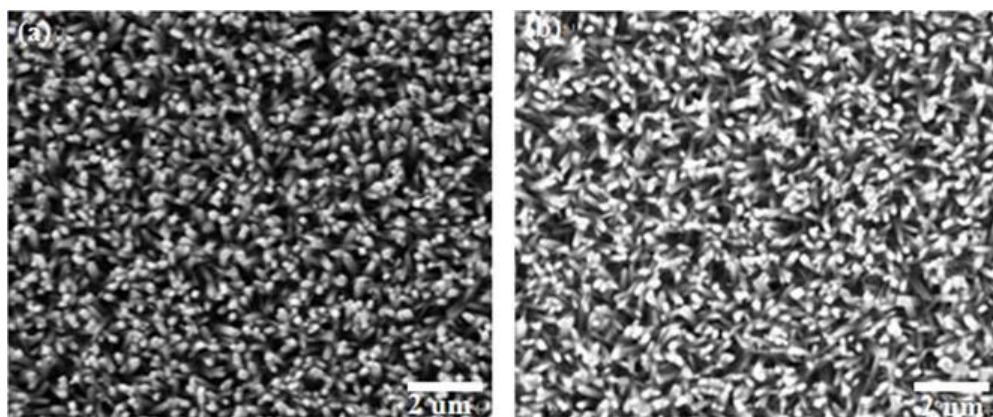
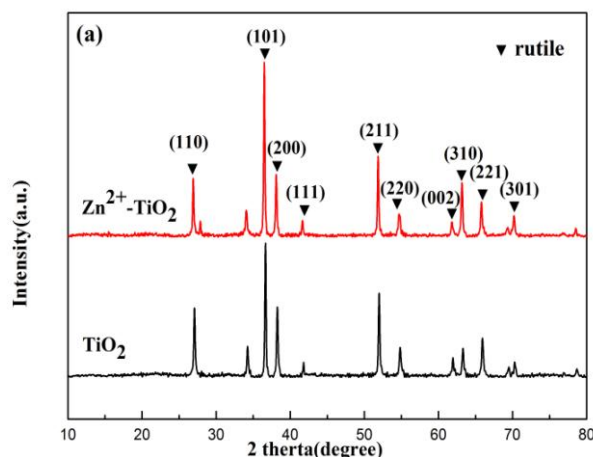


Figure 1. (a) and (b) FESEM images of top view section of pure TNRs

As shown in Fig.2, the rutile structure of TiO_2 was detected in the case of the mixed oxides. A more detailed analysis of the XRD results from Fig.2 demonstrates that the peak maxima shift toward smaller angles when increasing the Zn^{2+} concentration. As an instance, the peak at $34^\circ < 2\theta < 40^\circ$ is presented both for pure TNRs and for mixed oxide with 2 mmol $(CH_3COO)_2Zn$ doped in Fig.2. This phenomenon clearly indicates that the Zn^{2+} is well distributed in the whole nanocrystal and only parts of them doping might cause slight changes of lattice constant. We notice that a similar result has been reported in a recent investigation [29]. According to the Bragg equation, the author indicates the intensity of the diffraction peaks enhances gradually with the increase of doping concentration because of the distinctions of radius, which is consistent with our results and supposition.



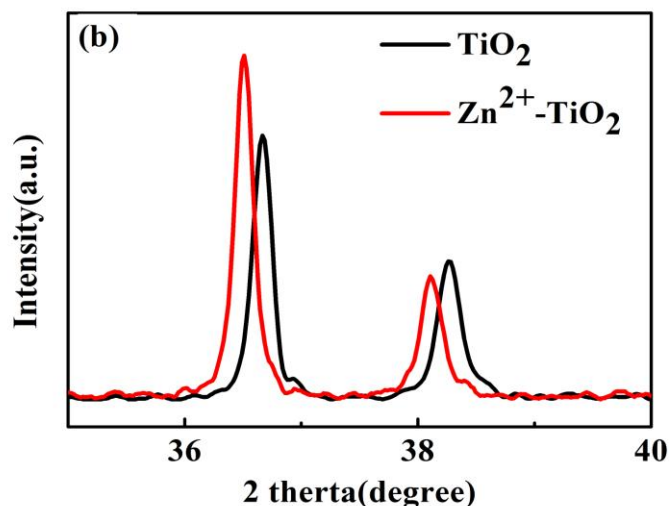
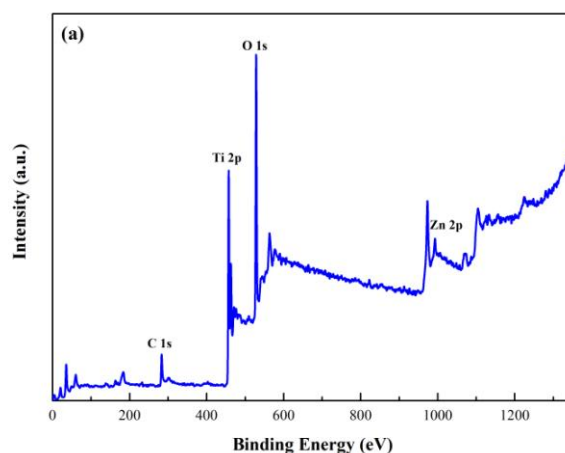


Figure 2. (a) XRD patterns of pure TNRs, and Zn^{2+} -doped TNRs. (b) Detailed XRD patterns ($34^\circ < 2\theta < 40^\circ$).

To give a further analysis on the chemical components and possible variations of the binding energies of Ti and O after doping Zn^{2+} , we collected the results of Zn 2p, Ti 2p and O 1s levels utilizing the XPS technique. Fig.3a shows the XPS survey spectrum of TNRs with 2 mmol Zn^{2+} doped including the elements of Ti, O, C and Zn. There are doublet peaks of Zn 2p observed at the binding energy between 950 and 1050 eV (Fig. 3a). In addition, the high resolution peaks for Ti 2p (Fig. 3b) and for O 1s (Fig. 3c) also shows remarkable changes after doping Zn^{2+} . At the same time, compared with the theoretical binding energies of pure TNRs (458.6 eV for $\text{Ti}2p_{3/2}$ and 464.4 eV for $\text{Ti}2p_{1/2}$, 529.4eV for O1s), the binding energies of Zn^{2+} -TNRs slightly shifted toward lower levels (457.08 eV for $\text{Ti}2p_{3/2}$, 462.88eV for $\text{Ti}2p_{1/2}$ and 528.28eV for O 1s), respectively corresponding to the decrease of 1.52 eV and 1.12 eV. The lower energy trends of Ti and O binding energies after doping Zn^{2+} , as well as the similar angle shift of (101) peak in the XRD pattern, strongly provide convincing evidence for the successful combination of Zn^{2+} and the TiO_2 matrix.



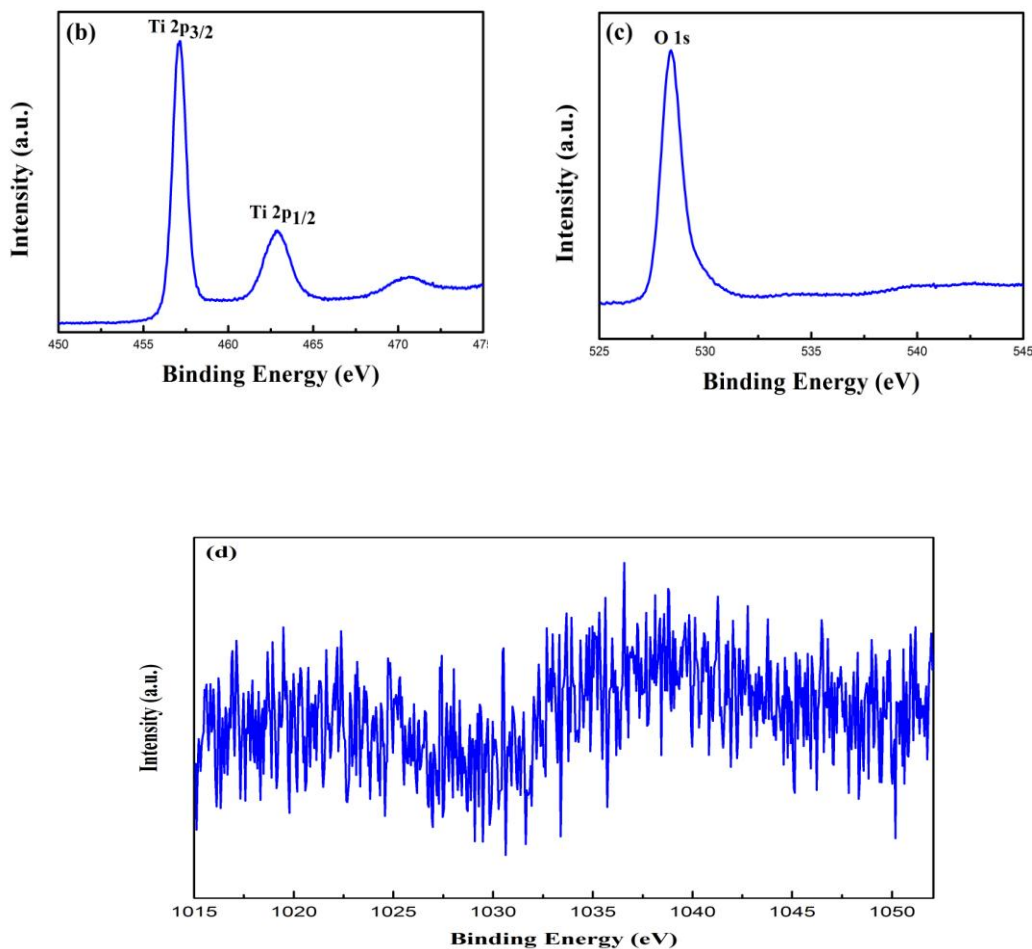


Figure 3. (a) XPS patterns of the TiO₂ nanorod with 2 mmol Zn²⁺ doped. (b,c and d) Narrow scanning XPS patterns of Ti 2p, O 1s and Zn 2p

Table 1. Detailed information of XPS patterns

Name	Peak BE	Area (P)	Atomic %
Ti2p	457.14	325945.2	21.73
O1s	528.42	307108.2	56.87
C1s	283.28	43055.1	21.39
Zn2p	993.08	-	<0.01

Furthermore, according to Fig.3a, d and Table 1, what deserves to be mentioned is that just an imperceptible amount of Zn²⁺ (atomic% < 0.01%) participated in the doping process even though total (CH₃COO)₂Zn consumption in our experiments was relative higher.

3.2 Optical properties

The UV-visible spectra of the Zn²⁺-TNRs are to determine the relationship between energy conversion efficiency and spectroscopic property, shown in Fig. 4. The absorption band for the

tetrahedral symmetry of Ti^{4+} usually appears at approximately 380 nm. In the spectra, compared with pure TNRs, the absorption bands of Zn^{2+} -TNRs were obviously red-shifted. The band gaps in semiconductors are reported to link closely to the absorbed wavelength range [30], where the band gap lessens with rising absorption wavelength. The above results indicate that the addition of Zn^{2+} did alter the band gap of the TiO_2 semiconductor significantly. Moreover, a similar tendency was reported by adopting other ions into TNRs [31]. In accordance with the Mie theory [32], the particle size of anodic materials as a light scattering layer is comparable to wavelength of lights. Otherwise, small particles will probably lead to Rayleigh scattering which is not strong enough to scatter lights. In this case, Zn^{2+} -TNRs are supposed to have relative larger size than pure TNRs to produce a multi-reflection of incident light which matches the result of XRD above mentioned.

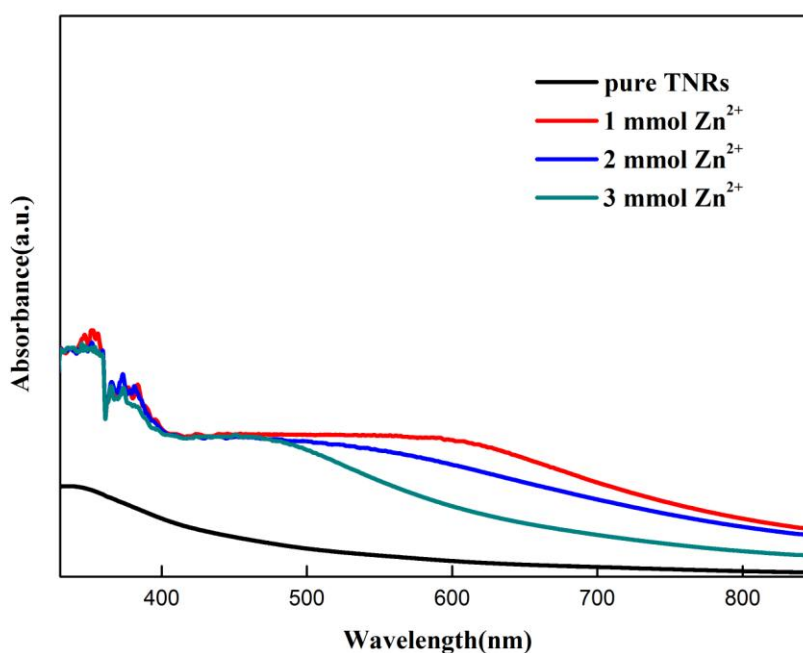


Figure 4. The UV-Vis curve of different DSSCs with Zn^{2+} doped

3.3 Photovoltaic performance

The internal resistances of the DSSCs were investigated via electrochemical impedance spectroscopy (EIS) in a range of frequencies from 10^{-2} to 10^5 Hz as well as the alternating current amplitude of 10 mV. Fig.5 shows the results of EIS at forward bias of the open-circuit voltage under light irradiation and the results are represented as Nyquist plots. Two semicircles dominate the whole curves, which correspond to charge transferring at the Pt/electrolyte and electrolyte/dye/ TiO_2 interfaces, respectively [33]. The relative low resistance of the Pt/electrolyte interface results in a not so obvious semicircle at the high frequency and the larger semicircle which corresponds to the electrolyte/dye/ TiO_2 interface appears at the lower frequency. Compared to the pure TNRs, the large

semicircles of DSSCs containing Zn^{2+} doping are much smaller. When the dosage of Zn^{2+} ascends, the resistance decreases and the smallest value is achieved at the sample doped with 2 mmol Zn^{2+} which also means the fastest electron transferring rate. However, further doping process (3mmol Zn^{2+}) leads to the increase of the resistance value even higher than that of the undoped one (shown in Table 2) which might indicate that the excessive doping process contributes to severe charge recombination at the electrolyte/dye/ TiO_2 interface.

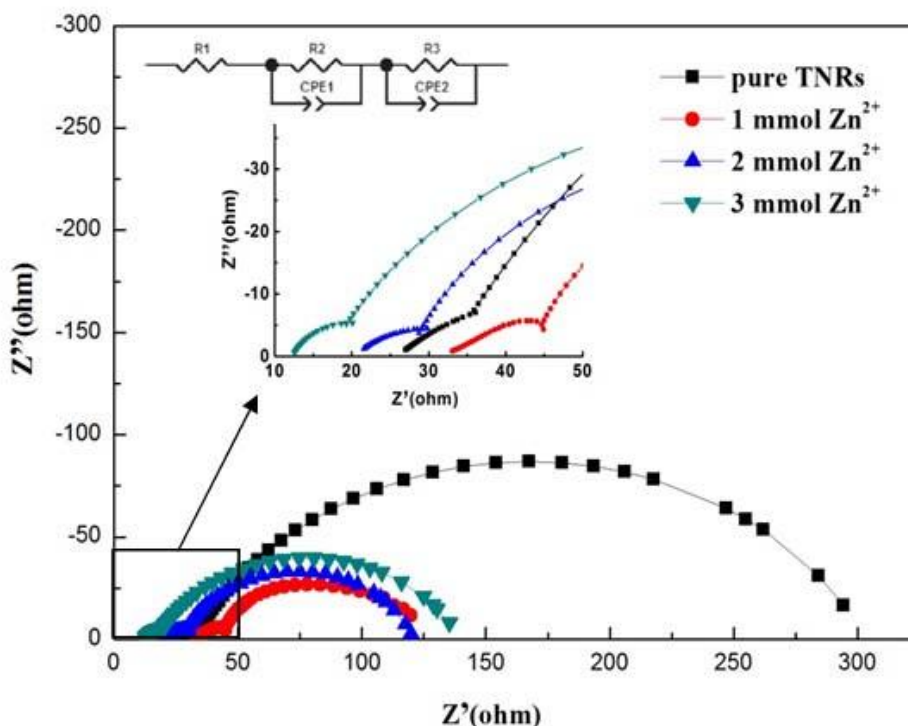
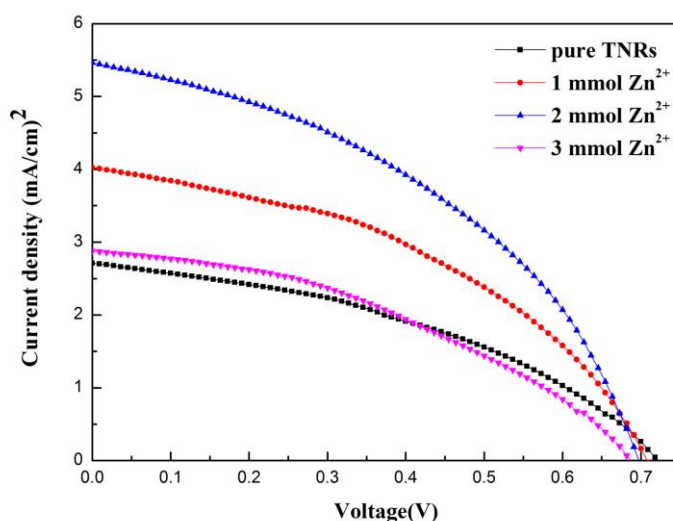


Figure 5. Nyquist plots of the DSSCs with different Zn^{2+} content from EIS in the frequencies ranging from 10^{-2} to 10^5 Hz under AM1.5 sunlight illumination of 100 mW/cm^2 . The inset indicates an equivalent circuit used for explaining the EIS results.

Fig. 6 shows the current density-voltage curves of the open cells based on Zn^{2+} -doped and pure TNRs. The average levels of their photoelectrical performance obtained from multiple cells with different Zn^{2+} concentration are summarized in Table 2. A distinct rise in the photocurrent for DSSCs was detected for doping levels from pure TNRs to 2 mmol Zn^{2+} doped TNRs. The energy-conversion efficiency of 1.61% was achieved for a DSSC with 2 mmol Zn^{2+} -doped TNRs, which was as twice as that of the undoped one. Nevertheless, a negative impact of doping Zn^{2+} in the photocurrent was observed in the sample of doping 3 mmol Zn^{2+} and energy-conversion efficiency was even lower than that of the one based on pure TNRs. It might indicate excessive Zn^{2+} doping lead to lattice distortion of TNRs which further changed the lattice and shifted the band gap of this composited structure and finally reduced the efficiency. This coincides with the indication of a related research, which explains that severe defects develop to recombination centers with a particularly high doping concentration and finally impede the charge transfer [29].

Table 2. Performances of DSSC composed of the as-prepared TiO₂ NR arrays with different content of Zn-doped

Growth conditions	Resistance (Ω)	Short-circuit current density (mA/cm^2)	Open-circuit voltage (V)	Fill factor	η (%)
Pure TNRs	257.9	2.73	0.72	0.41	0.8
1 mmol Zn ²⁺	90.9	4.05	0.71	0.42	1.21
2 mmol Zn ²⁺	71	5.44	0.69	0.43	1.61
3 mmol Zn ²⁺	117	2.87	0.68	0.40	0.78

**Figure 6.** The J-V curve of different DSSCs of Zn²⁺ doped

4. CONCLUSIONS

In summary, TiO₂ nanorod arrays are synthesized with a simple process using thermal hydrolysis. Furthermore, Zn²⁺ is dropped in TiO₂ nanorod arrays after the hydrolyzation of TBT and then successfully prepared Zn²⁺-TiO₂ nanorod arrays. The DSSCs using the Zn²⁺-TiO₂ nanorod arrays as the photo-anode demonstrate a high conversion efficiency of 1.61%, compared to 0.8% of those adopting pure TiO₂ nanorod arrays. The dropping of Zn²⁺ may cause lattice distortion of TiO₂ nanorod arrays and change the microspace of them. The efficiency enhancement is mainly attributed to the above mentioned special junction between Zn²⁺ and TiO₂ nanorod arrays which promote the absorption of dye and improve the transmission of electron. All these results indicate the proposed TNRs with Zn²⁺ doped photoanodes might be beneficial to improve the photoelectrical performance of DSSCs and has a promising prospect of application.

ACKNOWLEDGEMENTS

This work was financially supported by the Fundamental Research Funds for the Central Universities (2013QNB04).

References

1. B. O'Regan, M. Grätzel, *Nature* 353 (1991) 737.
2. M. Grätzel, *Acc. Chem. Res.* 42 (2009) 1788.
3. C.Y. Chen, M.K. Wang, J.Y. Li, N. Pootrakulchote, L. Alibabaei, C.H. Ngoc-Le, J.D. Decoppet, J.H. Tsai, C. Grätzel, C.G. Wu, S.M. Zakeeruddin, M. Grätzel, *ACS Nano* 3 (2009) 3103.
4. A. Yella, H.W. Lee, H.N. Tsao, C. Yi, A.K. Chandiran, Md.K. Nazeeruddin, E.W.-G. Diao, C.Y. Yeh, S.M. Zakeeruddin, M. Grätzel, *Science* 334 (2011) 629.
5. M.A. Green, K. Emery, Y. Hishikawa, W. Warta, *Prog. Photovolt. Res. Appl.* 19 (2011) 83.
6. P. V. Kamat, M. Haria, S. Hotchandani, *J. Phys. Chem. B* 108 (2004) 51.
7. X.P. Lin, D.M. Song, X.Q. Gu, Y.L. Zhao, Y.H. Qiang, *Appl. Surf. Sci.* 263 (2012) 816.
8. M. P. Char, E. Niranjana, B. E. K. Swamy, B. S. Sherigara and K. V. Pai, *Int. J. Electrochem. Sci.*, 3 (2008) 588.
9. J. M. Wu, T.W. Zhang, Y.W. Zeng, S. Hayakawa, K. Tsuru, A. Osaka, *Langmuir* 21 (2005) 6995.
10. X.W. Zeng, Y.X. Gan, E. Clark, L.S. Su, *J. Alloys Compd.* 509 (2011) 221.
11. M.Y. Guo, M.K. Fung, F. Fang, X.Y. Chen, A.M.C. Ng, A.B. Djurišić, W.K. Chan, *J. Alloys Compd.* 509 (2011) 1328.
12. M. Paulose, O.K. Varghese, G.K. Mor, C.A. Grimes, K.G. Ong, *Nanotechnology* 17 (2006) 398.
13. G.K. Mor, K. Shankar, M. Paulose, O.K. Varghese, C.A. Grimes, *Nano Lett.* 5 (2005) 191.
14. X.J. Feng, K. Shankar, O.K. Varghese, M.P. Paulose, T.J. Latempa, C.A. Grimes, *Nano Lett.* 8 (2008) 3781.
15. C. Zhu, M. Shi, S.C. Yang, H. Zhang, Z.M. Yang, B.J. Ding, *J. Alloys Compd.* 485 (2009) 328.
16. O.K. Varghese, M.P. Paulose, C.A. Grimes, *Nature Nanotechnol.* 4 (2009) 592.
17. E. Enache-Pommoler, B. Liu, E.S. Aydil, *Phys. Chem. Chem. Phys.* 11 (2009) 9648.
18. M.J. Yang, B. Ding, S.W. Lee, J.K. Lee, *J. Phys. Chem. C* 115 (2011) 14534.
19. Q.L. Huang, G. Zhou, L. Fang, L.P. Hu, Z.S. Wang, *Energy Environ. Sci.* 4 (2011) 2145.
20. Z. Yu, X. Li, X. Wang, J. Li and K. Cao, *Int. J. Electrochem. Sci.*, 6 (2011) 3890.
21. B. Liu, E.S. Aydil, *J. Am. Chem. Soc.* 131 (2009) 3985.
22. Y. Zhang, Y. Gao, X.H. Xia, Q.R. Deng, M.L. Guo, L. Wan, G. Shao, *Mater. Lett.* 64 (2010) 1614.
23. R.H. Tao, J.M. Wu, H.X. Xue, X.M. Song, X. Pan, X.Q. Fang, X.D. Fang, S.Y. Dai, *J. Power Sources* 195 (2010) 2989.
24. X.J. Lu, X.L. Mou, J.J. Wu, D.W. Zhang, L.L. Zhang, F.Q. Huang, F.F. Xu, S.M. Huang, *Adv. Funct. Mater.* 20 (2010) 509.
25. J.C. Lee, T.G. Kim, W. Lee, S.H. Han, Y.M. Sun, *Cryst. Growth Des.* 9 (2009), 4519.
26. H. Wang, Y.S. Bai, H. Zhang, Z.H. Zhang, J.H. Li, L. Guo, *J. Phys. Chem. C* 114 (2010), 16451.
27. J.H. Bang, P.V. Kamat, *Adv. Funct. Mater.* 20 (2010), 1970.
28. M. Li, Y. Liu, H. Wang, H. Shen, W.X. Zhao, H. Huang, C.L. Liang, *J. Appl. Phys.* 108 (2010), 094304.
29. Xujie Lü, Xinliang Mou, Jianjun Wu, Dingwen Zhang, Linlin Zhang, Fuqiang Huang, Fangfang Xu, Sumei Huang, *Adv. Funct. Mater.* 2010, 20, 509-515
30. Zhu, Y.L. Zhao, X.P. Lin, X.Q. Gu, Y. H. Qiang, *Superlattice Microst.* 65 (2014) 152.
31. Jinho Chae, Dong Young Kim, Sujung Kim, Misook Kang, *J. Ind. Eng. Chem.* 16 (2010) 906-911
32. G.T. Dai, L. Zhao, J. Li, W. Li, F. Hu, Z.X. Xu, B.H. Dong, H.B. Lu, S.M. Wang, J.G. Yu, *J. Colloid Interf. Sci.* 365 (2012) 46.L.
33. V.S. Saji, M. Pyo, *Thin Solid Films* 518 (2010) 6542.